Synthetic and Systems Biotechnology 8 (2023) 772–783

Contents lists available at ScienceDirect

Synthetic and Systems Biotechnology

journal homepage: www.keaipublishing.com/en/journals/synthetic-and-systems-biotechnology

Original Research Article

Enzymatic properties and inhibition tolerance analysis of key enzymes in β-phenylethanol anabolic pathway of *Saccharomyces cerevisiae* HJ

Qilin Yang [a,d,1], Shuangping Liu [a,b,c,d,**,1], Yuzong Zhao [a,d], Xiao Han [a,b,c,d], Rui Chang [a,d], Jian Mao [a,b,c,d,*]

[a] National Engineering Research Center of Cereal Fermentation and Food Biomanufacturing, State Key Laboratory of Food Science and Technology, School of Food Science and Technology, Jiangnan University, Wuxi, Jiangsu, 214122, China
[b] Shaoxing Key Laboratory of Traditional Fermentation Food and Human Health, Jiangnan University (Shaoxing) Industrial Technology Research Institute, Shaoxing, Zhejiang, 312000, China
[c] National Engineering Research Center of Huangjiu, Zhejiang Guyuelongshan Shaoxing Wine Co., Ltd., Shaoxing, Zhejiang, 312000, China
[d] Jiangsu Provincial Engineering Research Center for Bioactive Product Processing Technology, Jiangnan University, Wuxi, Jiangsu, 214122, China

ARTICLE INFO

Keywords:
Ehrlich pathway
Phenylalanine aminotransferase and phenylpyruvate decarboxylase
Saccharomyces cerevisiae
Metabolic engineering
Escherichia coli

ABSTRACT

Huangjiu is known for its unique aroma, primarily attributed to its high concentration of β-phenylethanol (ranging from 40 to 130 mg/L). Phenylalanine aminotransferase Aro9p and phenylpyruvate decarboxylase Aro10p are key enzymes in the β-phenylethanol synthetic pathway of *Saccharomyces cerevisiae* HJ. This study examined the enzymatic properties of these two enzymes derived from *S. cerevisiae* HJ and S288C. After substrate docking, Aro9p^{HJ} (−24.05 kJ/mol) and Aro10p^{HJ} (−14.33 kJ/mol) exhibited lower binding free energies compared to Aro9p^{S288C} (−21.93 kJ/mol) and Aro10p^{S288C} (−12.84 kJ/mol). *ARO9* and *ARO10* genes were heterologously expressed in *E. coli* BL21. Aro9p, which was purified via affinity chromatography, showed inhibition by L-phenylalanine (L-PHE), but the reaction rate V_{max}(Aro9p^{HJ}: 23.89 μmol·(min•g)$^{-1}$) > Aro9p^{S288C}: 21.3 μmol·(min•g)$^{-1}$) and inhibition constant K_i values (Aro9p^{HJ}: 0.28 mol L^{-1}>Aro9p^{S288C} 0.26 mol L^{-1}) indicated that Aro9p from *S. cerevisiae* HJ was more tolerant to substrate stress during *Huangjiu* fermentation. In the presence of the same substrate phenylpyruvate (PPY), Aro10p^{HJ} exhibited a stronger affinity than Aro10p^{S288C}. Furthermore, Aro9p^{HJ} and Aro10p^{HJ} were slightly more tolerant to the final metabolites β-phenylethanol and ethanol, respectively, compared to those from S288C. The study suggests that the mutations in Aro9p^{HJ} and Aro10p^{HJ} may contribute to the increased β-phenylethanol concentration in *Huangjiu*. This is the first study investigating enzyme tolerance mechanisms in terms of substrate and product, providing a theoretical basis for the regulation of the β-phenylethanol metabolic pathway.

1. Introduction

Huangjiu is fermented by adding wheat *qu* and some enzyme preparation, yeast, and other saccharifying starters, such as alcohol, aldehyde, ester, acid, and other substances, to enrich the body of *Huangjiu* mellow and typica [1,2]. As one of the aromatic alcohols, β-phenylethanol is one of the main by-products produced by *Saccharomyces cerevisiae* during the brewing process of *Huangjiu* [3,4]. The content of β-phenylethanol in *Huangjiu* is 40 mg/L-130 mg/L β-phenylethanol to a certain extent enhances the flavor of seasonings such as *Huangjiu* and other fermented foods, thereby positively impacting their sensory characteristics [5]. However, when its concentration is excessively high, it may potentially pose negative effects on the human body. Therefore, understanding the metabolic regulation mechanisms of β-phenylethanol is crucial for healthy consumption of such products.

The aromatic alcohols in *Huangjiu* are mainly produced by

Peer review under responsibility of KeAi Communications Co., Ltd.
* Corresponding author. National Engineering Research Center of Cereal Fermentation and Food Biomanufacturing, State Key Laboratory of Food Science and Technology, School of Food Science and Technology, Jiangnan University, Wuxi, Jiangsu, 214122, China.
** Corresponding author. National Engineering Research Center of Cereal Fermentation and Food Biomanufacturing, State Key Laboratory of Food Science and Technology, School of Food Science and Technology, Jiangnan University, Wuxi, Jiangsu, 214122, China.
E-mail addresses: liushuangping668@126.com (S. Liu), maojian@jiangnan.edu.cn (J. Mao).
[1] Qilin Yang and Shuangping Liu and contributed equally to this work.

https://doi.org/10.1016/j.synbio.2023.11.006
Received 11 September 2023; Received in revised form 14 November 2023; Accepted 15 November 2023
Available online 28 November 2023

S. cerevisiae, and their concentration is highly positively correlated with the concentration of ethanol. Previous studies on promoter strength and two-dimensional gene expression analysis show that aromantic alcohol biosynthesis of *S. cerevisiae* is primarily based on the *Ehrlich* pathway. The concentration of total aromatic alcohols produced by *S. cerevisiae* HJ01 was higher than that of the model strain [6].

A series of enzymes in the Shikimic acid and *Ehrlich* pathways catalyze the synthesis of β-phenylethanol by *S. cerevisiae* [7,8]. In the *Ehrlich* pathway, *S. cerevisiae* transaminates L-phenylalanine (L-PHE) in the presence of phenylalanine aminotransferase to form phenylpyruvate (PPY), and decarboxylase decarboxylates the decarboxylation of carboxyl to form phenylacetaldehyde. Finally, β-phenylethanol is reduced to β-phenylethanol by dehydrogenase [9,10], the other is the Shikimic acid pathway. However, little is known about the biosynthetic pathway of aromatic alcohols in *Huangjiu* fermentation and the key enzymes involved in this process. In our previous studies, two key enzymes have been isolated, purified, and characterized from *S. cerevisiae* HJ and *S. cerevisiae* S288C. Mutations in PDT (I161K, L239P, and Q250H) were identified in *S. cerevisiae* HJ01. Pha2p^{HJ} exhibited higher substrate affinity (K_m, 11.1 mM–15.9 mM), catalytic efficiency, and thermal stability but was less sensitive to feedback inhibition. Therefore, the PDT mutation of *S. cerevisiae* HJ01 leads to a higher concentration of β-phenylethanol in *Huangjiu*. There were four amino acid differences (58 (V-T), 127(Q-E), 147(Q-E), and 151(I–V)) in the active catalytic region of alcohol dehydrogenase Adh1p [11], which led to a higher tolerance to β-phenylethanol and ethanol of yeast strain Adh1p^{HJ} than Adh1p^{S288C}.

Transaminization is the rate-limiting step in the *Ehrlich* pathway, and the *ARO10* gene mainly determines phenylpyruvate decarboxylase activity and that PPY will be preferentially catalyzed by the *ARO10*-encoded enzyme during reaction [12,13]. Many studies have shown a close link between enzyme expression and aromatic alcohol production in beer and wine [14]. By overexpressing *ARO80*, *ARO9*, and *ARO10* genes simultaneously, the concentration of β-phenylethanol produced by *S. cerevisiae* was increased threefold. *ARO80* is a crucial transcription factor in the aromatic alcohol synthesis pathway [15]. Therefore, it is essential to explore the phenylalanine aminotransferase and phenylpyruvate decarboxylase encoded by *ARO9* and *ARO10* genes in *huangjiu* (Fig. 1).

In this study, our aim was to enhance the understanding of the enzyme regulatory mechanism involved in the key biosynthetic pathway of β-phenylethanol - the Ehrlich pathway, during *Huangjiu* fermentation. We primarily investigated the structure, enzymatic properties and kinetics of Aro9p and Aro10p from *S. cerevisiae* HJ and model strain S288C, with a particular focus on the mechanisms of substrate and end product resistance [16].

2. Materials and methods

2.1. Reagents

Sodium dodecyl sulfate (SDS), Histrap™ HP column, and molecular mass markers were obtained from GE Healthcare Life Sciences (Sweden). β-mercaptoethanol, kanamycin, and IPTG were obtained from Sigma-Aldrich. All chemicals were of analytical grade and commercially available.

2.2. Strains, plasmids, and materials

Strain *S. cerevisiae* HJ was isolated from the traditional *Huangjiu* fermentation process at Zhejiang Guyuelongshan Shaoxing Wine Co., Ltd., the largest *Huangjiu* producer in the world, as a β-phenylethanol producing yeast strain. *S. cerevisiae* S288C was used as the comparator strain (Table 1). The genomic DNA of *S. cerevisiae* and *ARO9* and *ARO10* were prepared according to our previous reports [17]. The primers for *ARO9* amplification were GGGAATTCCATATGATGACTGCTGGTTCT GTCCC, which contained a *Nde* I site (underlined), and CGAGCTCT-CAACTTTTATAGTTGTCAA, which contained a *Sac* I site (underlined). And the primers for *ARO10* amplification were GGGAATTCCA-TATGATGGCACCTGTTACAATTGA, which ontained a *Nde* I site (underlined), and GGATCCCTATTTTTTATTTCTTTTAA, which ontained a *Bam*H I site (underlined). The PCR products were ligated with vector pESI-T and then digested by *Nde* I and *Sac* I(*Bam*H I). The resulting fragment was ligated with similarly restricted pET-28a (+) to construct pET-28a-*ARO9*^{S288C} and pET-28a-*ARO9*^{HJ}, pET-28a-*ARO10*^{S288C} and

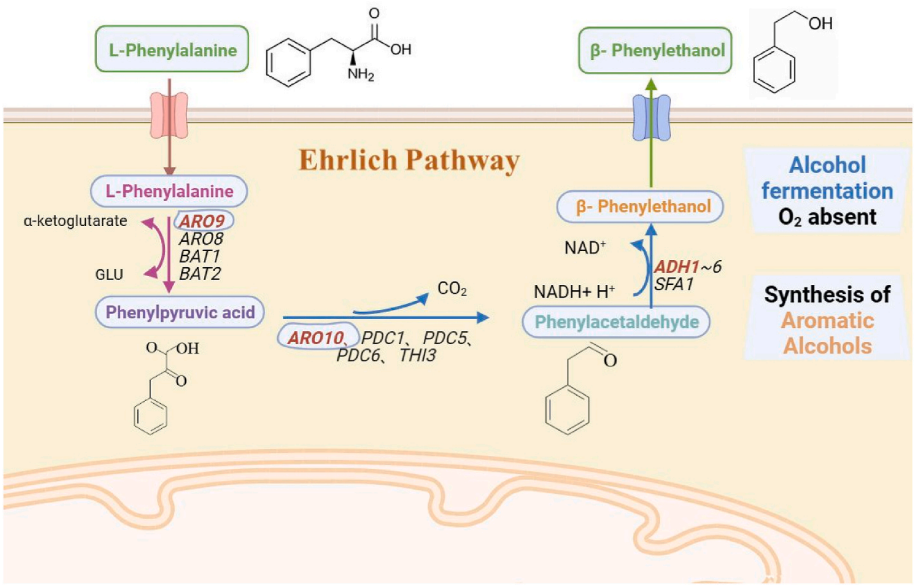

Fig. 1. Phenylalanine aminotransferase and phenylpyruvate decarboxylase of the Ehrlich pathway of *S. cerevisiae*
Aromatic amino acid aminotransferase I and aromatic amino acid aminotransferase II, both of which belong to the first family of aminotransferases, are encoded and synthesized by genes *ARO8* and *ARO9*, respectively. Through the research and comparison of genes, it is found that the amino acid difference between Aro8p^{HJ} and Aro8p^{S288C} is located at the edge of the protein structure, so it will not be studied for the time being (data not shown). According to previous studies, *PDC1*, *PDC5*, *PDC6*, and *THI3* mainly encode pyruvate decarboxylase, and the activity of phenylpyruvate decarboxylase is mainly determined by the *ARO10* gene. Therefore, this study focused on *ARO9* and *ARO10*.

Table 1
Microbial strains and plasmids used in this study.

Strain and plasmids	Relevant characteristics	Source or reference
E. coli BL21(DE3)	F^- *ompT hsdS*$_B$ ($r_B^- m_B^-$) *gal dcm* (DE3)	Novagen
S. cerevisiae S288C	*MATα (leu2-3, can1-100,112 ura3-1 trp1-1, his3-11, ade2-1)*	ATCC 27325
S. cerevisiae HJ	*huangjiu* brewing yeast	*huangjiu* fermentation broth
pESI-T Vector	*amp*^{r}	TaKaRa, Japan
pET-28a(+)	*Kan*^{r} *lacI*	Novagen, USA
pET-28a-*ARO9*^{S288C}/ pET-28a-*ARO9*^{HJ}	*Kan*^{r} *lacI ARO9*^{S288C}/*ARO9*^{HJ}	This work
pET-28a-*ARO10*^{S288C}/ pET-28a-*ARO10*^{HJ}	*Kan*^{r} *lacI ARO10*^{S288C}/*ARO10*^{HJ}	This work

pESI-T Vecto is r as a cloning vector.
pET-28a (+) is used as a subcloning vector.

pET-28a-*ARO*10^{HJ}, respectively. These two plasmids were used individually to transform *E. coli* BL21(DE3), and Aro9p production was induced in the resulting strains with IPTG. TB medium (12 g/L tryptone, 24 g/L yeast extract, 5 g/L glycerol, 2.31 g/L KH_2PO_4 and 12.54 g/L K_2HPO_4) supplemented with kanamycin (30 mg/L) was used for protein production [18].

2.3. Sequence analysis and 3D structure analysis based on homology modeling

The *ARO9*^{HJ}and *ARO10*^{HJ} gene in plasmid pET-28a-*ARO9*^{HJ} and pET-28a-*ARO10*^{HJ} were sequenced by Sangon Biotech (Shanghai) Co., Ltd. The ProtParam tool (https://web.expasy.org/protparam/) was used to predict the molecular weight of genes through the amino acid sequence. The online tool TMHMM 2.0 (tool website: http://www.cbs.dtu.dk/services/TMHMM/) was used to predict transmembrane helices. The predicted three-dimensional (3D) structure of Aro9p^{HJ} was obtained using the Automated Mode in the SWISS-MODEL server (http://swissmodel.expasy.org/). The template sequence for the enzyme was obtained using the PDB (http://www1.rcsb.org/) database. A multiple sequence alignment of the deduced amino acid sequences of Aro9p^{S288C} and Aro9p^{HJ} the Aro9p from *Candida albicans* SC5314 was prepared using DNAMAN software. The structural models were viewed using PyMOL software [19].

Interactions between Aro9p (Aro10p) and L-PHE (PPY) were evaluated by a molecular docking study. 3D structures of ligands were retrieved from the PubChem database in SDF format. Molecular docking was carried out using AutoDock 4.2, and a grid box covering the 3D coordinates in X, Y, and Z-dimensions of active sites was created using AutoGrid. After a successful docking run, the conformation with the smallest binding energy was selected from the 100 results [20].

2.4. Protein expression, enzyme preparation, and purification

Pure enzymes were performed by metal-affinity chromatography. Firstly, When the optical density (OD) at 600 nm reached 0.6–0.8 (about 3–4 h), the cultures were cooled on ice, and gene expression was induced by the addition of 0.5 mM (0.4 mM) IPTG, and the mixture was cultured at 25 °C for an additional 12 h [5]. The biomass was harvested by centrifugation for 10 min at 12000 rpm and 4 °C. The resulting cell pellets were washed, and resuspended in PBS buffer (300 mM NaCl and 50 mM phosphate buffer at pH 8.0). Then the resuspended cells were incubated on ice for 20 min and lysed by sonication (Sonics Vibra - Cell) (300 W, 2 s, 1 s, Crushing time: 10 min). The crude extract was centrifuged at 12000 rpm for 30 min at 4 °C to remove cellular debris. As a control, *E. coli* BL21(DE3) cells harboring plasmid pET-28a (+) were treated similarly [21]. The crude extracts were used for activity determination and purification. Then the soluble portion was loaded on a Histrap™ HP chelated column connected to an AKTA avant 25 (GE Healthcare). The bound enzyme was eluted with 250 mM imidazole in 20 mM phosphate buffer (pH 7.0). Enzyme solutions were desalted and stored at 4 °C until further use [22].

2.5. Enzyme assays

2.5.1. Enzyme assays of phenylalanine aminotransferase Aro9p

The reaction mixture (1 mL) consisted of potassium dihydrogen phosphate buffer (0.1 mmol L^{-1}, pH 8.0), pyridoxine phosphate (0.1 mmol L^{-1}), L-phenylalanine (1 mmol L^{-1}), pyruvate (10 mmol L^{-1}) as amino receptor, and enzyme (0.2 mg protein-0.6 mg protein). The reaction started with the addition of L-phenylalanine. When 1 mL of 1 mol L^{-1} sodium hydroxide was added to the ice surface and reacted at 30 °C for 2 min and 10 min, the two parallel reactions of transaminase activity stopped. PPY, the reaction product of phenylalanine aminotransferase, was determined at 320 nm. The assay was carried out at least in triplicate [23].

$$U\ /\ (\mu mol/min) = \frac{V \bullet \triangle A_{320}}{t \bullet \varepsilon \bullet b} \times 100$$

In the formula, V was the volume of the reaction system (mL); $\triangle A_{320}$ was the absorbance difference; t was reaction time (min); The ε is in mole extinction coefficient (17.5×10^3 L (mol·min)$^{-1}$); b was the optical path (cm); The enzyme activity unit (U) of one phenylalanine aminotransferase was defined as the amount of enzyme required to produce 1 μmo1 product PPY within 1min. Specific enzyme activity (U•g^{-1}) was defined as the unit of enzyme activity per g of phenylalanine aminotransferase Aro9p [24].

2.5.2. Enzyme assays of phenylpyruvate decarboxylase Aro10p

The activity of phenylpyruvate decarboxylase was determined by coupled optical analysis assisted by alcohol dehydrogenase, and the activity of phenylpyruvate decarboxylase was determined by consuming NADH at 340 nm. The assay system was as follows: 200 μL reaction system: containing sodium phosphate (20 mmol L^{-1}, pH 7.0), ThDP (0.2 mmol L^{-1}), Mg^{2+} (0.1 mmol l^{-1}), NADH (0.35 mmol L^{-1}), yeast alcohol dehydrogenase(1 U•mL^{-1}). The reaction started with the addition of pure enzyme (40 μL, 50 μg mL^{-1}) and reacted at 37 °C for 15 min. The activity of phenylpyruvate decarboxylase was determined by monitoring the reduction of NAD^+ at 340 nm. The calculation formula is as follows [25]:

$$U\ /\ (\mu mol/min) = \frac{V \bullet \triangle A_{340}}{t \bullet \varepsilon \bullet b} \times 100$$

A unit of phenylpyruvate decarboxylase activity (U) is defined as the amount of enzyme required to reduce 1 μmo1 of coenzyme NADH in 1 min. The specific enzyme activity(U•g^{-1}) was defined as the enzyme activity unit per g of phenylpyruvate decarboxylase Aro10p [26].

2.6. Enzyme characterization and kinetics

2.6.1. Effect of temperature on activity and stability of the purified enzyme

The optimal temperature of purified Aro9p (Aro10p) was determined at temperatures ranging from 15 °C to 70 °C. For thermal stability, residual activity was determined after incubation by the value of the temperature range employed for 1 h using L-PHE(PPY) as substrate at 40 °C and pH 7.0. The experiment was performed in triplicate [27].

2.6.2. Effect of pH on activity and stability of the purified enzyme

The optimal pH of purified Aro9p (Aro10p) was determined using L-PHE (PPY) as substrate in 20 mM sodium phosphate-sodium citrate (pH 3.0–8.0) and 20 mM sodium carbonate-sodium bicarbonate (pH 9.0–10.0). For pH stability, the residual activity was measured at 40 °C and pH 6.0 using L-PHE(PPY) as substrate after incubation at various pH values for 1 h. The experiment was performed in triplicate [18].

2.6.3. Kinetic parameter analysis and effectiveness factor

The kinetic parameters of Aro9p (Aro10p), such as the maximum velocity (V_{max}), Michaelis-Menten constant (K_m), turnover number (k_{cat}), and catalytic efficiency (k_{cat}/K_m), were determined after calculating the activity in the presence of different concentrations (0 mmol L^{-1} - 5 mmol L^{-1} substrate) at the optimum temperature and pH. A Lineweaver-Burk plot of 1/v versus 1/s was employed for the V_{max} and K_m calculations. The data were fitted to the linear model using a double-reciprocal plot. K_m is the value of the Michaelis–Menten constant without the presence of the inhibitor. Inhibition Constant K_i was calculated with reference to previous studies [28].

2.7. Statistical analysis

Origin Pro 9.0 software (OriginLab Corp., Northampton, MA, USA) was used for data sorting and calculation and atlas production, and Prism7.0 software (GraphPad Software, San Diego, CA) software was used for significance analysis. Except for special instructions, three parallels were set for each sample, and data were expressed as mean ± standard deviation.

3. Results

3.1. Sequence and structural analysis

3.1.1. Sequence and structural analysis

Physicochemical characterizations of proteins are closely related to their structures, which can lay the foundation for studying their functions and interactions with small molecules. Physicochemical parameters such as pI, amino acid composition, instability index, amino acid hydrophilicity, hydrophobicity, etc., were analyzed for the Aro9p and Aro10p. This could provide a reference for predicting the advanced structure of the protein [29]. The Prot Param program, based on a sequence of enzyme bioinformatics prediction, found that the molecular formula of $Aro9p^{HJ}$ and $Aro10p^{HJ}$ were $C_{2645}H_{4072}N_{676}O_{786}S_{19}$ and $C_{3176}H_{4931}N_{833}O_{948}S_{26}$, respectively, and the molecular weight were 58.53 kDa and 70.79 kDa. The total number of atoms were 8198 and 9914, and the computed pI value were 5.27 and 5.76 (pI < 7). This suggests that the protease is least soluble when the pH of the solution is at its isoelectric point [30]. The total number of basic amino acid residues (Arg + Lys) were 55 and 59, less than those of acidic amino acid residues (Asp + Glu), which were 66 and 70, indicating that phenylalanine aminotransferase $Aro9p^{HJ}$ and phenylpyruvate decarboxylase Aro10p are acidic protein. The Grand Average Hydropathy (GRAVY) values were found to be −0.322 and −0.183. These negative GRAVY values suggest that these proteins could exhibit better interaction with water (hydrophilic in nature) [31].

3.1.2. Homology modeling analysis and substrate molecular docking study

The open reading frames of $Aro9p^{HJ}$ and $Aro9p^{S288C}$ both encompass 1542 base pairs, encoding protein sequences of 513 amino acids each. According to a BLAST analysis against the UniProt database and homology modeling using the SWISS-MODEL, these two proteins exhibit the highest amino acid identities of 37.97 % and 38.35 % respectively, to the aromatic aminotransferase Aro9 from *Candida albicans*(PDB ID:6HND) [32]. The tertiary structure of these proteins provides important insights into their functional molecular mechanisms. Homology-based protein modeling is an effective computational tool for predicting the structure of unknown proteins based on the determined 3D structures of other proteins in the same family that have similar folds and/or functions [33]. The homology modeling prototypes of $Aro9p^{HJ}$ and $Aro9p^{S288C}$ were determined to be aromatic-amino-acid: 2-oxoglutarate transaminase from *Candida albicans* SC5314. As shown in Fig. 2 (A and C), the structure of Aro9p includes a dimer of 59 kDa protein subunits, each consisting of 513 amino acids. This is similar to the structure of *CaAro9p* [32]. The N-terminal region of phenylalanine aminotransferase Aro9p contains two antiparallel β-folded sheets. These are distinct characteristics of Aro9p that differ from other transaminases and are related to the formation of the Aro9p dimer [34].

The enzymes Aro9p catalyzes the interconversion of amino acids and oxoacids through a transfer of amino groups. Aminotransferases utilized pyridoxal-5′-phosphate (PLP) as a coenzyme to transit the amino groups. Sequence analysis revealed noticeable differences between amino acids 12 (T-A), 79 (N-D), 454 (L-V), and 460 (V-L) in $Aro9p^{HJ}$ and $Aro9p^{S288C}$, which are located in the unconserved region. The Center Grid box coordinates were set as (X: 65.506, Y: 39.431, Z: 13.620), and the small molecule compound (L-PHE) connected to the binding site of Aro9p, as shown in Fig. 2B and D. In general, the configuration with the lowest docking energy was chosen as the most likely binding conformation. In this case, the minimum $Aro9p^{HJ}$ docking score was −24.05 kJ/mol, with docking in $Aro9p^{HJ}$ - PHE compounds found in the ASN144, PHE168, ASN232, LYS317, ARG324, ARG481, GLY50(from the other subunit), TYR102(from the other subunit), and ARG347(also from the other subunit) residues as the essential residues. The minimum $Aro9p^{S288C}$ docking score was −21.93 kJ/mol, with docking in $Aro9p^{S288C}$ - PHE compounds found in the ASN 144, PHE168, PRO170, ASN232, LYS317, ARG324, PHE426, ARG481, LYS32 (from the other subunit), GLY50 (also from the other subunit), TYR102 (also from the other subunit), and ARG347 (also from the other subunit) residues as the critical residues. These results could assist in understanding the enzyme's conformational specificity and illustrate the superior spontaneous binding of the substrate (L-PHE) to $Aro9p^{HJ}$.

Simultaneously, both $Aro10p^{HJ}$ and $Aro10p^{S288C}$ are coded by open reading frames of 1908 base pairs, which encode amino acid sequences of 635 residues each. The BLAST analysis compared to the UniProt database and homology modeling against the SWISS-MODEL revealed that these two sequences have the highest amino acid identity of 34.92 % and 34.95 % respectively, to the pyruvate decarboxylase from *S. cerevisiae* (PDB ID:2W93) [35]. This suggests that the homologous modeling prototypes for $Aro10p^{HJ}$ and $Aro10p^{S288C}$ are derived from the pyruvate decarboxylase of *S. cerevisiae*. The enzymatic function of Aro10p relies on the thiamine diphosphate (ThDP) cofactor, which primarily binds to the protein component at the interface via a divalent metal ion, typically magnesium. Pyruvate decarboxylases are enzymes composed of multiple subunits, with a typical subunit having a molecular weight between 59 kDa and 61 kDa (Fig. 3A and C). The tetramer is the catalytically active form of most PDCs [26,36]. Based on the crystal structure of ScPDC, it is hypothesized that only in the tetrameric state can the intermediate (R-) domain, which is very flexible and contains C221, interact with other domains in the other subunits [35,36]. Sequence analysis revealed that the notable difference in amino acids 377 (A-V) and 527 (K–R) between $Aro10p^{HJ}$ and $Aro10p^{S288C}$ was located in the unconserved region (Fig. 3F).

Amino acid residues at the active site directly interact with substrates attached to the C2 atom of the cofactor, substantially increasing enzyme catalysis speed. Therefore, the C2 position of ThDP was used as the grid box center (X: 12.927, Y: 17.033, Z: 24.852). The small molecule compound (PPY) was connected to the binding site of Aro10p, as shown in (Fig. 3B and D). In this situation, the lowest $Aro10p^{HJ}$ docking score was −14.33 kJ/mol, with $Aro10p^{HJ}$ - PPY compounds revealing Glu334, Ile335, Thr444, Gly445, Gln448, Phe449, Leu469, Ile544, Ile548, Leu621, Met624, Val625, Ala628 residues as key residues. The lowest $Aro10p^{S288C}$ docking score was −12.84 kJ/mol, with the key residues near the ligand in the docked $Aro10p^{S288C}$ – PPY compounds being identical to those in the $Aro10p^{HJ}$ - PPY compounds. These results could assist in understanding the enzyme's conformational specificity and illustrate the better spontaneous binding of the substrate (PPY) to $Aro10p^{HJ}$.

In summary, sequence analysis showed that the amino acid mutation in $Aro9p^{HJ}$ and $Aro10p^{HJ}$ might be one of the reasons for the better spontaneous binding of substrate (L-PHE or PPY) to enzyme. The results might be elucidated further through the study of enzymology properties

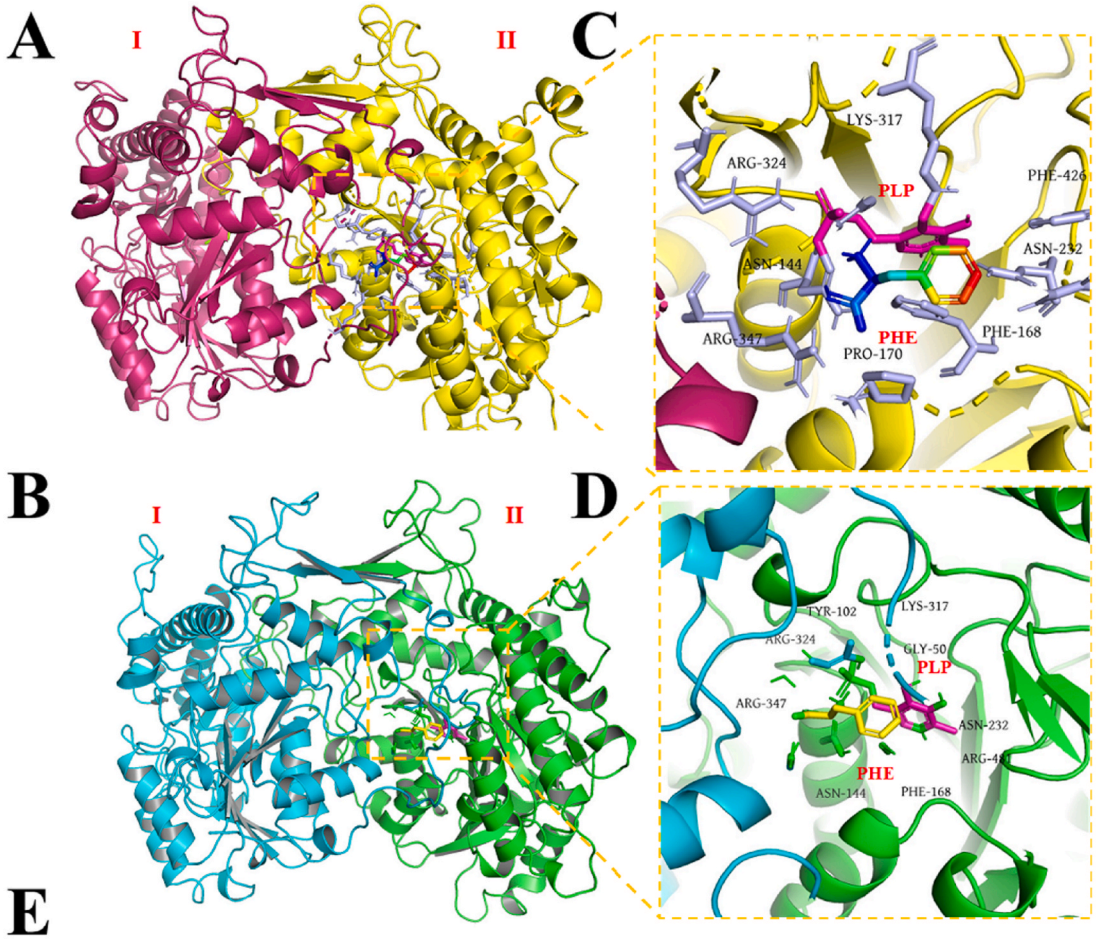

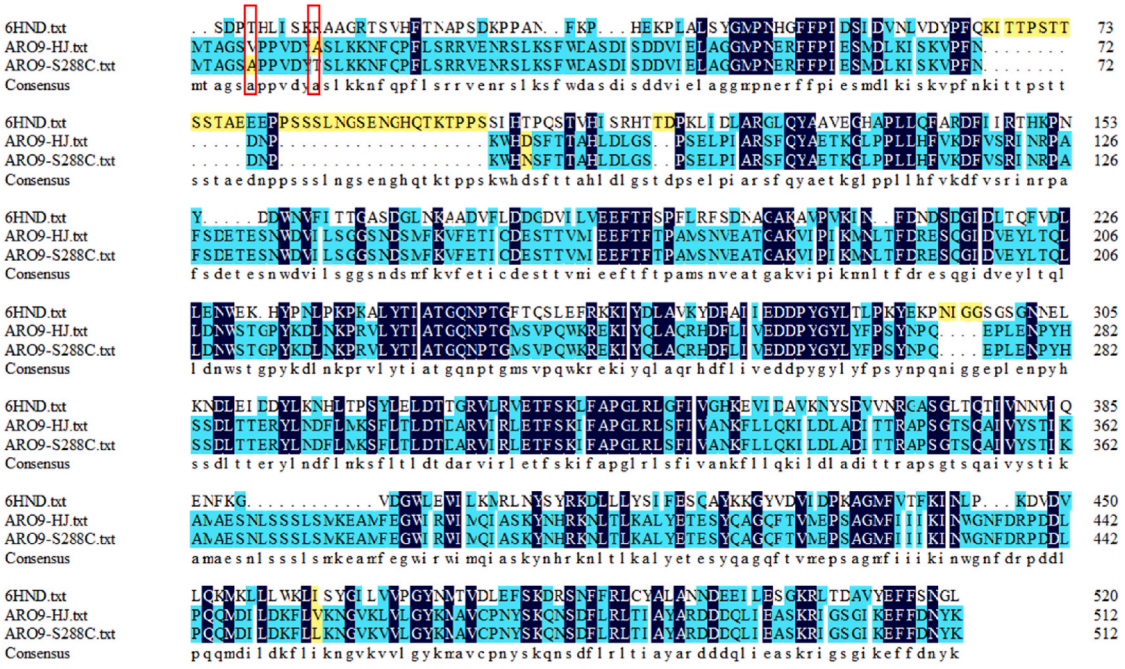

Fig. 2. The sequences and structures of phenylalanine aminotransferase Aro9p An L-PHE residue is bound covalently (forming an external aldimine) to the PLP cofactor in the ligand-binding cavity of Aro9p. Residues of subunits I and II surround the L-PHE ligand. Aro9p^{S288C} -dimer (A); Aro9p^{HJ} -dimer (B); L-PHE bound to Aro9p^{S288C} (C); L-PHE bound to Aro9p^{HJ} (D); Multiple alignments of amino acid sequences of phenylalanine aminotransferase Aro9p from *Candida albicans* SC5314. (PDB ID: 6HND), *S. cerevisiae* HJ(*ARO9*-HJ), and *S. cerevisiae* S288C(*ARO9*-S288C) (E). Aro9p^{S288C}: NP_012005.1; *ARO9*^{S288C}: GENE ID:856539.

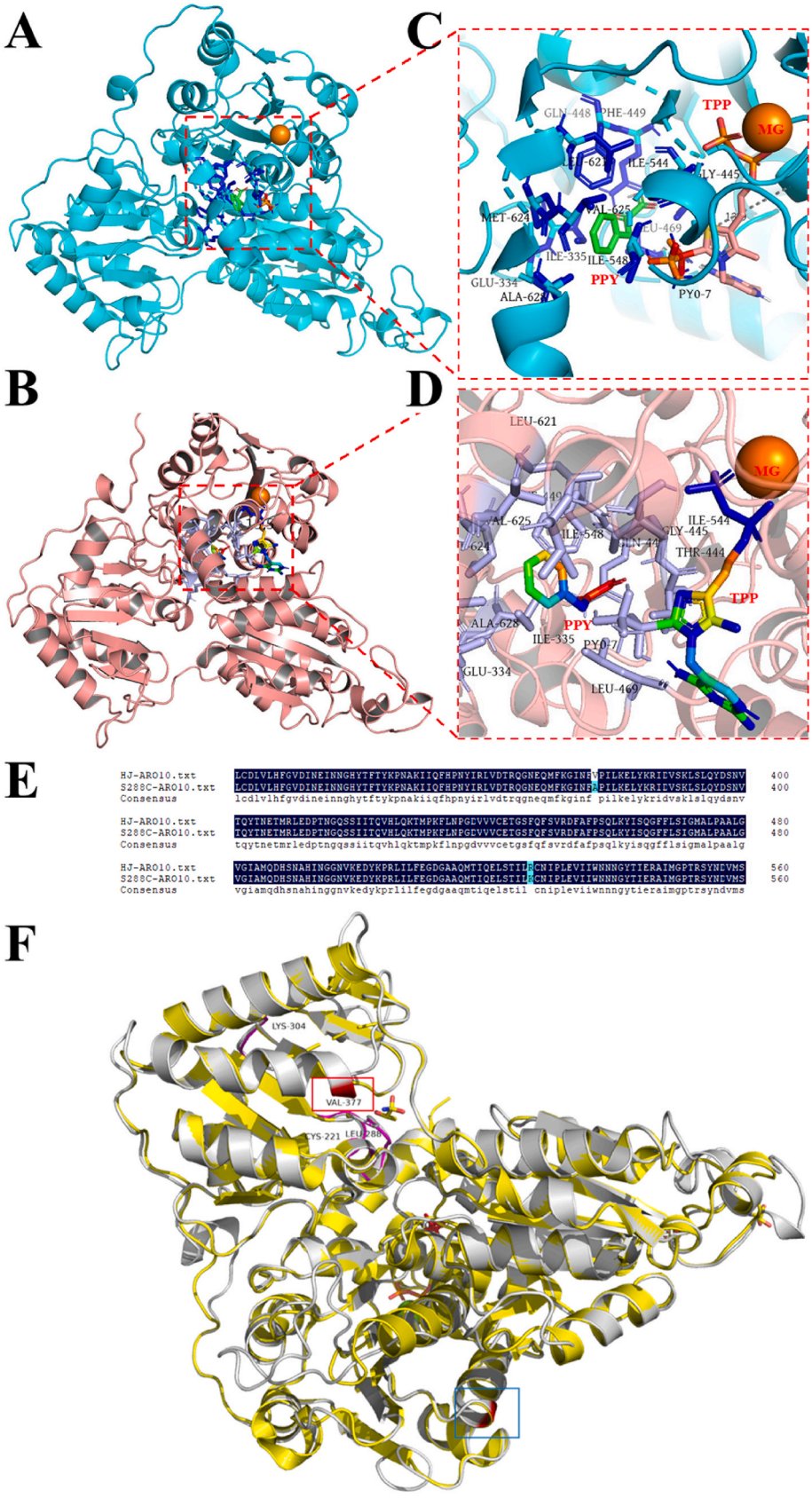

Fig. 3. The sequences and structures of pyruvate decarboxylase Aro10p
PPY residue is bound covalently (forming an external aldimine) to the PPY cofactor in the ligand-binding cavity of Aro10p. Aro10p^{S288C} - monomer (A); Aro10p^{HJ} - monomer (B); PPY bound to Aro10p^{S288C} (C); PPY bound to Aro10p^{HJ} (D); Multiple alignments of amino acid sequences of pyruvate decarboxylase Aro9p from *S. cerevisiae* HJ(*ARO10*-HJ), and *S. cerevisiae* S288C(*ARO10*-S288C) (E). Mapping of amino acid differences (Yellow: 2W93; Grey: Aro10p^{HJ}; Magentic red: structural loop 288–304 and the enzyme regulatory site C221; Red: amino acids of Aro10p^{HJ} V377 and R527) (F); Aro10p^{S288C}: NP_010668.3; *ARO10*^{S288C}: GENE ID:851987.

in experimental analysis.

3.2. Gene expression and enzyme purification

ARO9 (1542 bp) and *ARO10* (1928 bp) genes (Figs. S1A and D) were amplified and cloned into pET28a-*ARO9* and pET28a-*ARO10* plasmids, respectively, and transformed to *E. coli* BL21 (DE3). Plasmid maps are shown in Figs. S1B and E. The recombinant plasmids were verified by restriction endonucleases and sequenced by Shanghai Sangon.

The *ARO9* and *ARO10* gene encoding 514 and 635 amino acids respectively, are expressed in recombinant bacteria, resulting in proteins with molecular weights of 58.53 kDa and 70.79 kDa. In short, the prepared IPTGs were added to TB liquid mediums until the final concentrations were 0.5 mmol L^{-1} and 0.4 mmol L^{-1}, induced at 25 °C for 14 h and 12 h, and then the bacteria were centrifuged to obtain the precipitated thallus. The results were shown in Figs. S2A and C, characteristic bands appeared at about 60 kDa and 72 kDa which were consistent with the expected molecular weight of the designed protein [36].

The crude enzyme solutions were crushed by centrifugation, and the supernatants were pretreated with 0.22 μm membrane. Affinity chromatography was used to separate and purify the target proteins, and the eluents at peak positions were collected (Figs. S2B and E). The protein distributions were analyzed using SDS-PAGE, showing molecular weights approximately 60 kDa and 72 kDa, which were close to the predicted molecular weights of the recombinant enzymes, indicating successful overexpression and purification of phenylalanine aminotransferase Aro9p and phenylpyruvate decarboxylase Aro10p in *E. coli* strains (Figs. S2C and F).

3.3. Biochemical characterization of Aro9p

The pH and temperature characteristics of the phenylalanine aminotransferase Aro9p were studied. The experimental results showed that the optimal reaction pH of phenylalanine aminotransferase Aro9p was 6.0. The results were shown in Fig. 4A. In the range of pH 3.0–6.0, the enzyme activity increased; when the pH was greater than 6.0, the enzyme activity gradually weakened. The most stable pH of Aro9p was 7.0. Fig. 4B showed that after 1h incubation of phenylalanine aminotransferase Aro9p in the range of pH 7.0–8.0, more than 80 % of the enzyme activity remained, and the enzyme activity of $Aro9p^{HJ}$ was slightly higher than that of $Aro9p^{S288C}$. The residual enzyme activity of $Aro9p^{S288C}$ was less than 40 % after 1 h incubation in a buffer of pH 3.0–5.0. It also indicated that phenylalanine aminotransferase Aro9p was relatively stable under neutral pH conditions.

The results showed that the optimum reaction temperature of phenylalanine aminotransferase Aro9p was 30 °C, and the enzyme activity of $Aro9p^{HJ}$ (17.86 U g^{-1}) was similar to that of $Aro9p^{S288C}$ (17.61 U g^{-1}). The results were shown in Fig. 4E. Within the range of 15 °C–30 °C, and the enzyme activity increased with the increase in temperature. When the temperature was higher than 30 °C, the enzyme activity decreased relatively quickly. The most stable temperature of Aro9p was 30 °C. Fig. 4F showed that after incubation at 15 °C–30 °C for 2 h, the enzyme activity of phenylalanine aminotransferase Aro9p was still more than 60 %. When the temperature was higher than 30 °C, the enzyme activity began to weaken, and when the temperature was higher than 60 °C, the remaining enzyme activity was less than 40 %.

According to some relevant studies, aromatic amino acid transaminase (AAATs) from *Proteus mirabilis* JN458, a key enzyme in the β-phenethyl alcohol synthesis pathway, exhibits high enzyme activity at temperatures ranging from 30 to 50 °C and pH levels between 6 and 9 [37]. The enzyme *VpAT* isolated from *Variovorax paradoxus* demonstrated high activity across a broad pH range (4–11.2) at 30 °C. At 55 °C, *VpAT* presents a maximum specific activity of 33 U mg^{-1}, approximately twice the specific activity at 30 °C [38]. For both PHE and LEU activities of aminotransferase from *Lactococcus*, the optimum temperature determined at pH8 ranged between 35 and 45 °C. Likewise, the activity of PDT, similar to that of *S. cerevisiae*, declined sharply in low pH conditions, suggesting that an acidic environment damages its activity [39].

3.4. Biochemical characterization of Aro10p

The experimental results showed that the optimal reaction pH of Aro10p was 7.0. The results were shown in Fig. 4C. The enzyme activity increased with the increase of pH within the range of 3.0–7.0 and gradually weakened when the pH was greater than 7.0. The most stable pH of Aro10p was 7.0. Fig. 4D showed that after incubation for 1h for phenylpyruvate decarboxylase Aro10p within the pH range of 7.0–8.0, more than 80 % of the enzyme activity remained, and the enzyme activity of $Aro10p^{HJ}$ was relatively slightly higher than that of $Aro10p^{S288C}$. The residual enzyme activity of $Aro10p^{S288C}$ was less than 40 % after 1h incubation in a buffer with pH 3.0–5.0.

The results showed that the optimum reaction temperature of Aro10p was 35 °C, and the specific enzyme activity of $Aro10p^{HJ}$ (77.81 U g^{-1}) was 25.49 % higher than that of $Aro10p^{S288C}$ (62.00 U g^{-1}). The results were shown in Fig. 4G. Within the range of 15 °C–40 °C, specific enzyme activity increased with the increase in temperature. When the temperature was higher than 40 °C, the relative enzyme activity decreased rapidly. The most stable temperature of Adh1p is 30 °C. Fig. 4H showed that after 1h incubation at 20–35 °C, more than 80 % of the enzyme activity remains. When the temperature was higher than 35 °C, the relative enzyme activity decreased rapidly, and when the temperature was higher than 60 °C, the remaining enzyme activity was less than 30 %.

The optimum pH of phenylpyruvate decarboxylase KDC4427 from *Bacterial Enterobacter* sp. CGMCC 5087 for substrate PPY was between 6 and 6.5, and the optimum temperature was 37 °C. KDC4427 was relatively stable between pH 6 and 8, but only 41 % of the residual activity was detected after incubation at 50 °C for 1 h [40].

3.5. Kinetic analysis

As depicted in Fig. 5, the reaction rate of $Aro9p^{HJ}$ (17.61 μmol·$(min•g)^{-1}$) was comparable to that of $Aro9p^{S288C}$ (17.86 μmol·$(min•g)^{-1}$) when the substrate concentration of L-PHE was 1 mM. However, when the substrate concentration of L-PHE reached 2 mM, the V_{max} reaction rate of $Aro9p^{HJ}$ (23.89 ± 1.35 μmol·$(min•g)^{-1}$) was 12.16 % higher than that of $Aro9p^{S288C}$ (21.3 ± 1.12 μmol·$(min•g)^{-1}$). The enzyme activity began to show some inhibition when the L-PHE concentration exceeded 2 mM.

Homology modeling results illustrated that CaAro9p from *C. albicans* was selected as the template for Aro9p. Unlike *S. cerevisiae*, CaAro9p demonstrated lower affinity for L-PHE (K_m: 4.76 ± 1.17 mM) than for L-TRP (K_m: 1.80 ± 0.18 mM). Moreover, the V_{max} reaction rate of CaAro9p (7.457 ± 457 μmol·$(min•g)^{-1}$) to L-PHE was lower than that of $Aro9p^{HJ}$ of *S. cerevisiae* HJ (23.89 μmol·$(min•g)^{-1}$). These characteristics may explain why *S. cerevisiae*, especially HJ, is more adept at utilizing L-PHE to produce PPY [41,42].

In terms of structure, the N-terminal domain is preceded by a 50-residue loop that extends over the surface of the other subunit, covering part of its substrate-binding site. There are amino acid differences in the N-terminal domain of $Aro9p^{HJ}$, $Aro9p^{S288C}$ and CaAro9p, located at the gating access position implicated in substrate entry into the active site. This might account for the varying affinity and reaction rates of the enzyme to the substrate.

In fact, there are also some studies on aromatic amino acid aminotransferase involved in β-phenylethanol biosynthesis in rose petal protoplasts. Under optimal pH and temperature conditions, recombinant RyAAAT3 revealed a V_{max} value for the conversion of L-PHE of 6.86 ± 0.04 nmol/mg protein/min [43]. $Aro9p^{HJ}$ of *S. cerevisiae* HJ might be more promising than rose petal protoplasts for further synthesis of β-phenylethanol from L-PHE [44].

Despite studies suggesting Aro9p is inhibited by the substrate keto

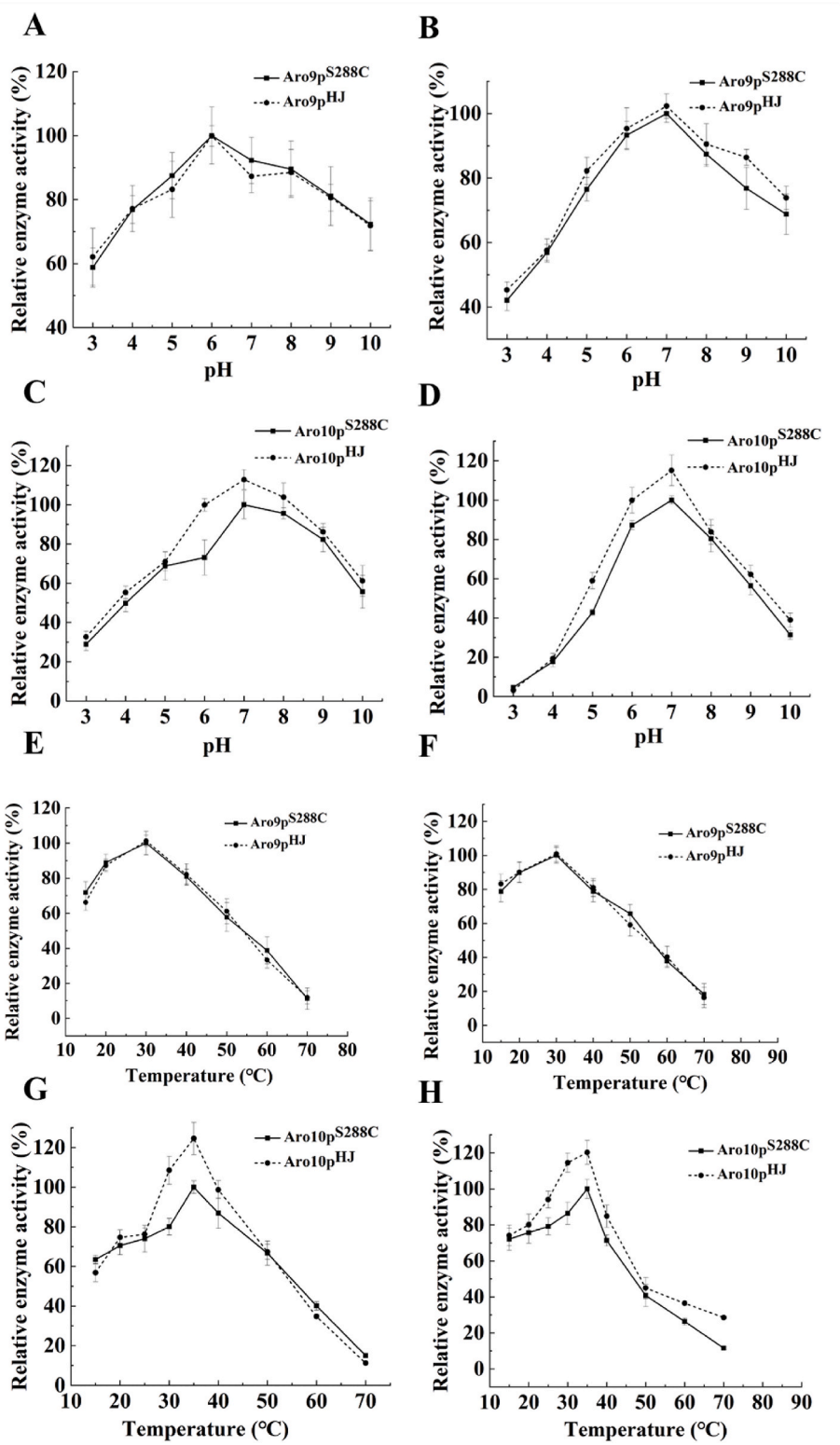

Fig. 4. Optimal pH and temperature for enzyme activity and stability of Aro9p and Aro10p
Relative enzyme activity under different pH reaction conditions of Aro9p(A); Stability of the enzyme Aro9p under different pH conditions (B); Relative enzyme activity under different pH reaction conditions of Aro10p(C); Stability of the enzyme Aro10p under different pH conditions (D); The relative Aro9p enzyme activity was measured at different temperature (E); The enzyme stability of Aro9p under different temperature (F); The relative Aro10p enzyme activity was measured at different temperature (G); The enzyme stability of Aro10p under different temperature (H).

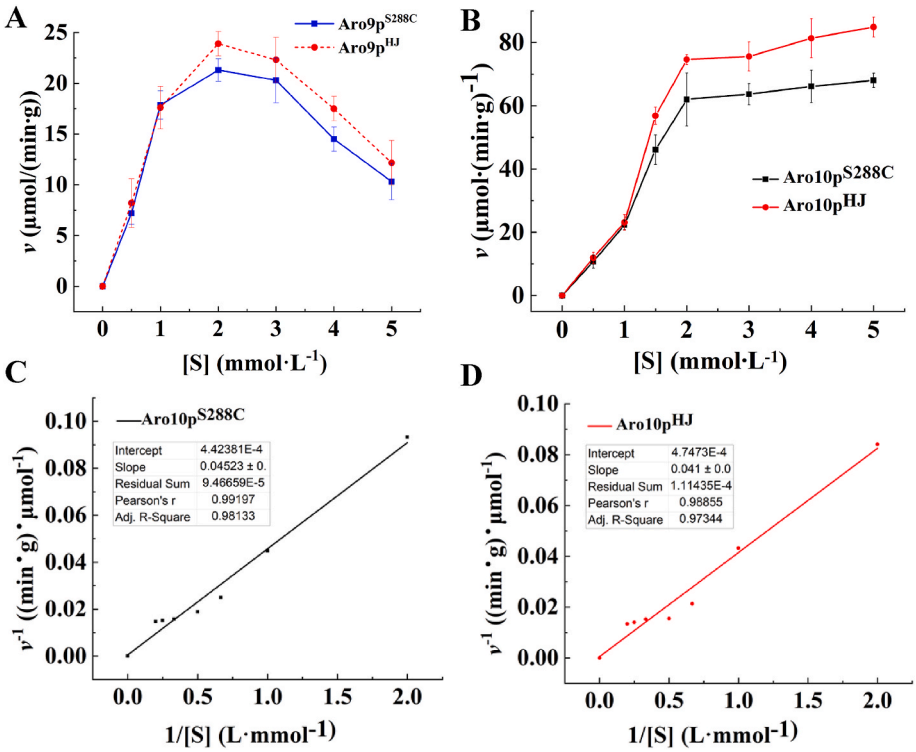

Fig. 5. Kinetic analysis of Aro9p and Aro10p
Non-linear regression of substrate and reaction rate of Aro9p(A); Non-linear regression of substrate and reaction rate of Aro10p(B); Relationship between 1/[S]-1/V of Aro10p^{S288C}(C); Relationship between 1/[S]-1/V of Aro10p^{HJ}(D).

acid, there have been few studies on the substrate inhibition of aromatic amino acid transaminase in the β-phenylethanol pathway. A series of experiments showed that the substrate inhibition constant showed that the K_i value of Aro9p^{HJ} (0.28 μmol L^{-1}) was higher than the K_i value of Aro9p^{S288C} (0.26 μmol L^{-1}). This indicates that Aro9p^{HJ} has greater resistance to substrate inhibition during catalysis, and higher catalytic efficiency (Fig. 5A). On a similar note, *Variovorax paradoxus* isolated from soil exhibits an aromatic β-amino acid aminotransferase, substrate inhibition also exists [38]. The apparent K_m and k_{cat} values (per monomer) for (S)-β-phenylalanine in the presence of 10 mM α-ketoglutarate were 1.5 mM and 11.8 s^{-1}, respectively, with an apparent substrate inhibition constant (K_i) of 40.3 mM. When using 10 mM (S)-β-phenylalanine, the apparent K_m and k_{cat} for α-ketoglutarate were 0.3 mM and 10.6 s^{-1}, respectively, with an apparent K_i of 82.4 mM. The larger K_i of VpAT for (S)-β-phenylalanine confirms that *VPAT* has a superior catalytic capacity for β-amino acids than for α-amino acids. In short, the higher K_i value of Aro9p^{HJ} compared with Aro9p^{S288C} may indicate that Aro9p^{HJ} is more resistant to L-PHE in the substrate inhibition study. This could potentially be due to changes in amino acid positions in the gating access.

With 0 mmol L^{-1}-5 mmol L^{-1} PPY as substrate, the initial reaction speed of phenylpyruvate decarboxylase Aro10p was measured, and the curve fitting was carried out with substrate concentration [*S*] as the X axis and speed *V* as the Y axis. As shown in Fig. 5B, with the increase of substrate concentration, phenylpyruvate decarboxylase Aro10p was saturated. Furthermore, the enzymatic kinetic results of Aro10p^{HJ} and Aro10p^{S288C} were analyzed, and the results were shown in Fig. 5. Finally, the Michaelis equation was obtained according to the data, and K_m, V_{max}, and k_{cat}/K_m values were obtained. As shown in Table 2, when PPY was used as the substrate, the K_m value of the characteristic constant of Aro10p^{S288C} (102.24 μmol L^{-1}) was larger than that of Aro10p^{HJ} (86.36 μmol L^{-1}), indicating that Aro10p^{HJ} had greater affinity with PPY than Aro10p^{S288C}. The V_{max} value of Aro10p^{HJ} (2106 μmol·(min•g)$^{-1}$) was 6.8 % lower than that of Aro10p^{S288C} (2260 μmol·(min•g)$^{-1}$). The value of k_{cat}/K_m (35.70 L (μmol•min)$^{-1}$) of Aro10p^{HJ} was equivalent to Aro10p^{S288C} (35.80 L (μmol•min)$^{-1}$), which indicated that the catalytic efficiency of Aro10p^{HJ} was equivalent to Aro10p^{S288C} under the same substrate PPY. However, Aro10p^{HJ} had a stronger affinity for PPY than Aro10p^{S288C}. Research indicates that during the grape juice fermentation process, for the substrate PPY, the V_{max} of ScAro10p was 3-fold higher than that of SkAro10p [21.7 ± 0.5 vs. 6.95 ± 0.15 nmol min^{-1} (mg protein) $^{-1}$] during wine fermentation. This mirrors our findings with Aro10p^{HJ}, where ScAro10p displayed robust catalytic capacity for PPY, a precursor of β-phenylethanol. The discrepancy could arise from the complexity of the synthetic must and the potential influence of other compounds on the formation of higher alcohols. Hence, Aro10p^{HJ} from *S. cerevisiae* HJ seems to showcase higher potential for the synthesis of aromatic alcohols such as β-phenylethanol from PPY [45].

Table 2
Analysis of Aro10p enzymatic parameters.

	Aro10p^{S288C}	Aro10p^{HJ}
V_{max} (μmol·(min•g)$^{-1}$)	2260.49 ± 7.54	2106.46 ± 5.14
K_m(μmol·L^{-1})	102.24 ± 2.15	86.36 ± 6.18
k_{cat}/K_m (L·(μmol•min)$^{-1}$)	35.8 ± 1.23	35.7 ± 2.01

3.6. The effects of ethanol and β-phenylethanol on enzyme activity and stability

The experimental results were shown in Fig. 6A. By exogenously adding 0 mg L^{-1} - 200 mg L^{-1} β-phenylethanol, the enzyme catalytic activity of phenylalanine aminotransferase Aro9p decreased with the increase of β-phenylethanol concentration, but the residual relative enzyme activity was more than 60 % and the expression of Aro9p^{HJ} with the increase of β-phenylethanol concentration. The tolerance to β-phenylethanol was stronger than that of Aro9p^{S288C}. When the

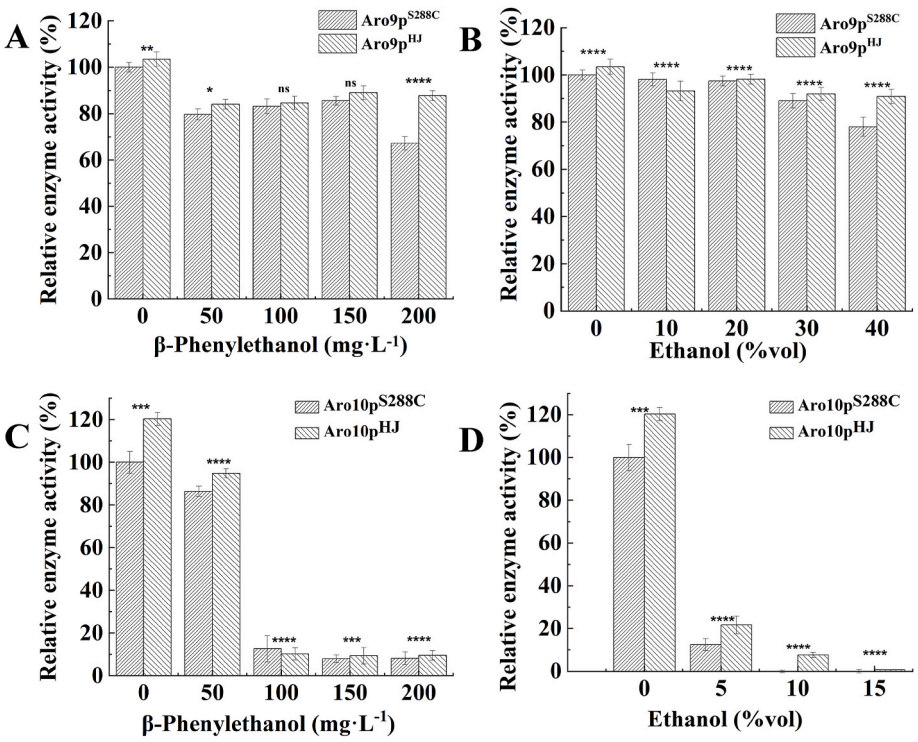

Fig. 6. Effect of exogenous end products on enzyme activity of Aro9p and Aro10p
β-phenylethanol was added to the assay system of enzyme Aro9p with L-PHE as substrate(A); Ethanol was added to the assay system of enzyme Aro9p with L-PHE as substrate(B); β-phenylethanol was added to the assay system of enzyme Aro10p with PPY as substrate(C); Ethanol was added to the assay system of enzyme Aro10p with PPY as substrate(D); *$P < 0.05$**$P < 0.01$*** It means $P < 0.001$**** It means $P < 0.0001$.

concentration of β-phenylethanol was 200 mg L^{-1}, the specific enzyme activity of phenylalanine aminotransferase $Aro9p^{HJ}$ (18.69 U g^{-1}) was 30.52 % higher than that of $Aro9p^{S288C}$. However, the catalytic activity of phenylalanine aminotransferase Aro9p on the substrate L-PHE decreased rapidly with the increase of alcohol content in the exogenous addition of 0%vol - 40%vol ethanol (Fig. 6B). The relative enzyme activity of $Aro9p^{HJ}$ remained 90.84 % in the addition of 40%vol ethanol. The relative enzyme activity of $Aro10p^{S288C}$ remained 78.02 %. In conclusion, β-phenylethanol and ethanol could inhibit the catalytic activity of phenylalanine aminotransferase Aro9p, but Aro9p was more stable under ethanol and β-phenylethanol.

The experimental results were shown in Fig. 6C. By exogenously adding 0 mg L^{-1} - 200 mg L^{-1} β-phenylethanol, the enzyme catalytic activity of phenylpyruvate decarboxylase Aro10p decreased rapidly with the increase of β-phenylethanol concentration. When the concentration of β-phenylethanol was 100 mg L^{-1}, the enzyme activity of phenylpyruvate decarboxylase Aro10p decreased to less than 20 %. In contrast, the tolerance ability of $Aro10p^{HJ}$ of *S. cerevisiae* HJ to β-phenylethanol was slightly higher than that of $Aro10p^{S288C}$. As shown in Fig. 6D with the increase of alcohol content, the catalytic activity of phenylpyruvate decarboxylase Aro10p for the decarboxylation reaction of the substrate phenylpyruvate also decreased rapidly. Under the condition of the addition of 5%vol ethanol, the relative enzyme activity of $Aro10p^{HJ}$ remained at 21.61 %. The relative enzyme activity of $Aro10p^{S288C}$ was only 12.45 %. In conclusion, β-phenylethanol and ethanol could inhibit the catalytic activity of phenylpyruvate decarboxylase Aro10p, and the ability of $Aro10p^{HJ}$ to tolerate β-phenylethanol and ethanol was slightly higher than that of $Aro10p^{S288C}$. The template ScPDC(2W93) of Aro10p from the previous homology modeling results has shown that there are two identified pathways for signal transfer during allosteric enzyme activation. The direct pathway begins at C221 and leads to the substrate binding site at ThDP via H92, E91, and W412. Structured loops 104–113 and 288–304 protect the active site from solvents, aided by the C-terminal helix. Intriguingly, the difference in amino acids at location 377 (A-V) is situated near their structural loop ScPDC(2W93) 288–304 and the enzyme regulatory site at C221 (Fig. 3F). It is plausible to hypothesize that this amino acid change restricts the effect of solvents (ethanol and β-phenethyl alcohol) on the enzyme Aro10p [5,25–27,45].

4. Discussion and conclusion

One of the reasons for the difference in aromatic alcohol content is the use of different yeast strains. Previous studies have shown that when the aromatic amino acid L-PHE is used as the sole nitrogen source, *S. cerevisiae* HJ produces more β-phenylethanol than S288C, indicating that there are differences in the enzyme activity of the pathways involved in the production of aromatic compounds [46].

The *Ehrlich* pathway is the main pathway for the production of β-phenylethanol during *Huangjiu* fermentation [14]. The phenylalanine transaminases, encoded by *ARO8* and *ARO9,* are crucial reversible enzymes that convert α-keto acids into aromatic amino acids [26]. However, the mechanism of how the catalytic direction changes unexpectedly, which plays an important role in the synthesis of aromatic alcohols, remains unclear. Previous studies have found that the promoter's strength for amino acid transaminase in *S. cerevisiae* HJ01 is weaker than that in the model strain S288C [6]. Aminotransferases are PLP-dependent enzymes that catalyze reversible transamination reactions between amino acids and α-ketoglutarate. Previous reports have shown that the enzyme activities of aminotransferases were affected by the product or substrate concentrations [38]. By analyzing the sequence information, we found four distinct amino acids (12(T-A), 79(N-D), 454 (L-V), and 460(V-L)) in $Aro9p^{S288C}$ and $Aro9p^{HJ}$. These differences might be located at the gated channel of the N-terminal domain, potentially influencing substrate entrance into the active site. This finding may partially explain why $Aro9p^{HJ}$, has a higher tolerance for substrate L-PHE and terminal metabolites (ethanol and β-phenylethanol) than $Aro9p^{S288C}$. Kinetic studies revealed that when the

concentration of substrate L-PHE reaches 2 mM, the reaction rate of Aro9p^{HJ} (23.89 μmol·(min•g)$^{-1}$) is 12.16 % higher than that of Aro9p^{S288C} (21.3 μmol (min•g)$^{-1}$). Also, the substrate inhibition constants show that the K_i value of Aro9p^{HJ} (0.28 mol L^{-1}) is higher than that of Aro9p^{S288C} (0.26 mol L^{-1}), indicating Aro9p^{HJ} more tolerant to substrate inhibition during the catalytic process and having a higher catalytic efficiency (Fig. 6A). This is also the first discovery of the potential of Aro9p^{HJ}, an aromatic amino acid transferase of industrial *S. cerevisiae* HJ from *Huangjiu* fermentation, for step-by-step conversion of L-PHE to produce aromatic alcohols such as β-phenylethanol [35]. In summary, Aro9p^{HJ} has a certain degree of tolerance to the substrate L-PHE and the product (ethanol and β-phenylethanol). Substrate inhibition may be an important mechanism for regulating *ARO9* enzyme activity and thus regulating the synthesis of aromatic alcohol metabolism in the *Ehrlich* pathway.

Phenylpyruvate decarboxylase exhibits independent α-keto acid decarboxylase activity, and in the reaction process, PPY is preferentially catalyzed by the enzyme encoded by *ARO10*. The promoter intensity of the *Ehrlich* pathway-related *ARO10* gene in *S. cerevisiae* HJ01 is significantly higher than that in the model strain of S288C [6]. Meanwhile, purified enzymatic characterization showed that the k_{cat}/K_m value of Aro10p^{HJ} (35.7 L (μmol•min)$^{-1}$) was comparable to that of Aro10p^{S288C} (35.8 L (μmol•min)$^{-1}$) under the same substrate PPY. However, Aro10p^{HJ} has a stronger affinity for PPY than Aro10p^{S288C}. Analysis of the effects of exogenous addition of terminal metabolites on enzyme activity showed that although β-phenylethanol and ethanol could seriously inhibit the catalytic activity of phenylpyruvate decarboxylase Aro10p, the ability of Aro10p^{HJ} to tolerate β-phenylethanol and ethanol was higher than that of *S. cerevisiae* Aro10p^{S288C}. The reason for this, perhaps the difference in amino acids 377 (A-V) is located near their structural loop ScPDC(2W93) 288–304 and enzyme regulatory site C221 (Fig. 3F) [8,14,15,24–26,45].

Since aromatic metabolism of yeast is strictly regulated, the tolerance mechanism of key enzymes can provide an effective method for the accumulation of related aromatic compounds. In addition, the synergistic effect of *ARO9* binding to *ARO10* is crucial and needs further study, such as the co-regulation of *ARO9* and *ARO10* on the effect of phenols reported by ZHU. In addition, after Sebastián M. Tapia proposed that changes in the *ARO80* gene may be meaningful for characterizing the regulatory domain of Aro80p, he intended to develop new strains that showed higher expression in *ARO9* and *ARO10* genes, thus increasing the yield of PE and PEA in wine. It can be seen that the key enzymes encoded by *ARO9* and *ARO10* genes are very important for regulating the metabolic synthesis of aromatic alcohols such as β-phenylethanol. To our knowledge, this report is the first to investigate the structural and enzymatic properties of the key enzymes Aro9p and Aro10p in the β-phenylethanol synthesis metabolic pathway of *Huangjiu* yeast. We also explored their tolerance mechanisms and found that these two key enzymes are less sensitive to inhibition by substrates or products, which may be one of the reasons why *Huangjiu* yeast produces a larger amount of β-phenylethanol. It lays a theoretical foundation for exploring the regulation of β-phenylethanol production by *Huangjiu* yeast. Furthermore, this study can also be used for research on the regulatory mechanism of other aromatic compounds.

CRediT authorship contribution statement

Qilin Yang: Investigation, Methodology, Data curation, Formal analysis, Writing – original draft. **Shuangping Liu:** Data curation, Formal analysis, Funding acquisition, Writing – review & editing. **Yuzong Zhao:** Resources, Project administration. **Xiao Han:** Methodology, Project administration. **Rui Chang:** Methodology, Resources. **Jian Mao:** Formal analysis, Funding acquisition.

Declaration of competing interest

The authors declare that they have no known competing financial interests or personal relationships that could have appeared to influence the work reported in this paper.

Acknowledgement

This work was financially supported by the National Natural Science Foundation of China (32072205, 22138004), and Shaoxing Science and Technology Plan Project (2022B43001).

Appendix A. Supplementary data

Supplementary data to this article can be found online at https://doi.org/10.1016/j.synbio.2023.11.006.

Abbreviations

L-PHE L-Phenylalanine;
PPY Phenylpyruvate
PLP Pyridoxal 5′-phosphate
ThDp Thiamine pyrophosphate
Aro9p^{HJ} Phenylalanine aminotransferase Aro9p from *Saccharomyces cerevisiae* HJ
Aro9p^{S288C} Phenylalanine aminotransferase Aro9p from *Saccharomyces cerevisiae* S288C
Aro10p^{HJ} Phenylpyruvate decarboxylase Aro10p from *Saccharomyces cerevisiae* HJ
Aro10p^{S288C} Phenylpyruvate decarboxylase Aro10p from *Saccharomyces cerevisiae* S288C

References

[1] Wang PX, Mao J, Meng XY, Li XZ, Liu YY, Feng H. Changes in flavour characteristics and bacterial diversity during the traditional fermentation of Chinese rice wines from Shaoxing region. Food Control 2014;44:58–63. https://doi.org/10.1016/j.foodcont.2014.03.018.
[2] Yang QL, Yao HL, Liu SP, Mao J. Interaction and application of molds and yeasts in Chinese fermented foods. Front Microbiol 2022;12. 3389.2021/fmicb.664850.
[3] Zhao YZ, Liu SP, Han X, Zhou ZL, Mao J. Combined effects of fermentation temperature and *Saccharomyces cerevisiae* strains on free amino acids, flavor substances, and undesirable secondary metabolites in *huangjiu* fermentation. Food Microbiol 2022;108. https://doi.org/10.1016/j.fm.2022.104091.
[4] Zhao Y, Liu S, Yang Q, Han X, Zhou Z, Mao J. *Saccharomyces cerevisiae* strains with low-yield higher alcohols and high-yield acetate esters improve the quality, drinking comfort and safety of *huangjiu*. Food Res Int 2022;161:111763. https://doi.org/10.1016/j.foodres.2022.111763.
[5] Liu SP, Yang QL, Mao JQ, Bai M, Zhou JD, Han X, Mao J. Feedback inhibition of the prephenate dehydratase from *Saccharomyces cerevisiae* and its mutation in *huangjiu* (Chinese rice wine) yeast. LWT–Food Sci Technol 2020;133. https://doi.org/10.1016/j.lwt.2020.110040.
[6] Liu SP, Bai M, Zhou JB, Jin ZM, Xu YZ, Yang QL, Zhou JD, Zhang SJ, Mao J. Analysis of genes from *Saccharomyces cerevisiae* HJ01 participating in aromatic alcohols biosynthesis during *huangjiu* fermentation. LWT–Food Sci Technol 2022;154. https://doi.org/10.1016/j.lwt.2021.112705.
[7] Xu W, Yang C, Xia Y, Zhang L, Liu C, Haiquan Y, Shen W, Chen X. High-level production of tyrosol with non-induced recombinant *Escherichia coli* by metabolic engineering. J Agric Food Chem 2020;68;16(4616):4623. https://doi.org/10.1021/acs.jafc.9b07610.
[8] Zhu L, Wang J, Xu S, Shi G. Improved aromatic alcohol production by strengthening the shikimate pathway in *Saccharomyces cerevisiae*. Process Biochem 2021;103:18–30. https://doi.org/10.1016/j.procbio.2021.01.025.
[9] Liang ZC, He B, Lin XZ, Su H, He ZG, Chen JX, Li WX, Zheng Y. Effect of *ADH7* gene loss on fusel oil metabolism of *Saccharomyces cerevisiae* for *Huangjiu* fermentation. LWT–Food Sci Technol 2023;175. https://doi.org/10.1016/j.lwt.2023.114444.
[10] Tian SF, Liang XL, Chen J, Zeng WZ, Zhou JW, Du GC. Enhancement of 2-phenylethanol production by a wild-type *Wickerhamomyces anomalus* strain isolated from rice wine. Bioresour Technol 2020;318. https://doi.org/10.1016/j.biortech.2020.124257.
[11] Yang QL, Liu SP, Zhao Y, Sun HL, Mao J. Heterologous expression and enzymatic analysis of alcohol dehydrogenase I in β-phenylethanol biosynthesis pathway from *huangjiu* yeast. J Chin Inst Food Sci Technol 2022;22(6):83–94. https://doi.org/10.16429/j.1009-7848.2022.06.009.
[12] Zhang CY, Qi YN, Ma HX, Li W, Dai LH, Xiao DG. Decreased production of higher alcohols by *Saccharomyces cerevisiae* for Chinese rice wine fermentation by deletion

of Bat aminotransferases. J Ind Microbiol Biotechnol 2015;42(4):617–25. 1007.10295/s015-1583-2015-z.
[13] Vuralhan Z, Morais M, Tai S, Piper M, Pronk J. Identification and characterization of phenylpyruvate decarboxylase genes in *Saccharomyces cerevisiae*. Appl Environ Microbiol 2003;69:4534–41. https://doi.org/10.1128/AEM.69.8.4534-4541.2003.
[14] Wang M, Sun Z, Wang Y, Wei Z, Chen B, Zhang H, Guo X, Xiao D. The effect of pitching rate on the production of higher alcohols by top-fermenting yeast in wheat beer fermentation. Ann Microbiol 2019;69(7):713–26. https://doi.org/10.1007/s13213-019-01463-w.
[15] Lee K, Sung C, Kim BG, Hahn JS. Activation of Aro80 transcription factor by heat-induced aromatic amino acid influx in *Saccharomyces cerevisiae*. Biochem Biophys Res Commun 2013;438(1):43–7. https://doi.org/10.1016/j.bbrc.2013.07.019.
[16] Xue YX, Chen XZ, Yang C, Chang JZ, Shen W, Fan Y. Engineering *Eschericha coli* for enhanced tyrosol production. J Agric Food Chem 2017;65(23):4708–14. https://doi.org/10.1021/acs.jafc.7b01369.
[17] Liu SP, Mao J, Liu YY, Meng XY, Ji ZW, Zhou ZL, Ai-lati A. Bacterial succession and the dynamics of volatile compounds during the fermentation of Chinese rice wine from Shaoxing region. World J Microbiol Biotechnol 2015;31(12):1907–21. https://doi.org/10.1007/s11274-015-1931-1.
[18] Yang S, Zhai L, Huang L, Meng D, Li J, Hao Z, Guan Z, Cai Y, Liao X. Mining of alkaline proteases from *Bacillus altitudinis* W3 for desensitization of milk proteins: their heterologous expression, purification, and characterization. Int J Biol Macromol 2020;153:1220–30. https://doi.org/10.1016/j.ijbiomac.2019.10.252.
[19] Agrawal S, Jana UK, Kango N. Heterologous expression and molecular modelling of L-asparaginase from *Bacillus subtilis* ETMC-2. Int J Biol Macromol 2021;192:28–37. https://doi.org/10.1016/j.ijbiomac.2021.09.186.
[20] Morris GM, Huey R, Lindstrom W, Sanner MF, Belew RK, Goodsell DS. Olson, A. J. AutoDock4 and AutoDockTools4: Automated docking with selective receptor flexibility. J Comput Chem 2009;30(16):2785–91. https://doi.org/10.1002/jcc.21256.
[21] Fan Y, Hua X, Zhang Y, Feng Y, Shen Q, Dong J, Zhao W, Zhang W, Jin Z, Yang R. Cloning, expression and structural stability of a cold-adapted β-galactosidase from *Rahnella sp.* R3. Protein Expr Purif 2015;115:158–64. https://doi.org/10.1016/j.pep.2015.07.001.
[22] Qin X, Xin Y, Su X, Wang X, Zhang J, Tu T, Wang Y, Yao B, Huang H, Luo H. Heterologous expression and characterization of thermostable chitinase and β-N-acetylhexosaminidase from *Caldicellulosiruptor acetigenus* and their synergistic action on the bioconversion of chitin into N-acetyl-d-glucosamine. Int J Biol Macromol 2021;192:250–7. https://doi.org/10.1016/j.ijbiomac.2021.09.204.
[23] Chen H, Huang H, Li X, Tong S, Niu L, Teng M. Crystallization and preliminary X-ray diffraction analysis of ARO9, an aromatic aminotransferase from *Saccharomyces cerevisiae*. Protein Pept Lett 2009;16(4):450–3. https://doi.org/10.2174/092986609787848036.
[24] Wang Z, Bai X, Guo X, He X. Regulation of crucial enzymes and transcription factors on 2-phenylethanol biosynthesis via Ehrlich pathway in *Saccharomyces cerevisiae*. J Ind Microbiol Biotechnol 2017;44(1):129–39. https://doi.org/10.1007/s10295-016-1852-5.
[25] Valera MJ, Zeida A, Boido E, Beltran G, Torija MJ, Mas A, Radi R, Dellacassa E, Carrau F. Genetic and transcriptomic evidences suggest *ARO10* genes are involved in benzenoid biosynthesis by yeast. Yeast 2020;37(9–10):427–35. https://doi.org/10.1002/yea.3508.
[26] Deed RC, Hou R, Kinzurik MI, Gardner RC, Fedrizzi B. The role of yeast *ARO8, ARO9* and *ARO10* genes in the biosynthesis of 3-(methylthio)-1-propanol from L-methionine during fermentation in synthetic grape medium. FEMS Yeast Res 2019;19(2). https://doi.org/10.1093/femsyr/foy109.
[27] Wang B, Bai Y, Fan T, Zheng X, Cai Y. Characterisation of a thiamine diphosphate-dependent alpha-keto acid decarboxylase from *Proteus mirabilis* JN458. Food Chem 2017;232:19–24. https://doi.org/10.1016/j.foodchem.2017.03.164.
[28] do Amaral M, Freitas ACO, Santos AS, Dos Santos EC, Ferreira MM, da Silva Gesteira A, Gramacho KP, Marinho-Prado JS, Pirovani CP. TcTI, a Kunitz-type trypsin inhibitor from cocoa associated with defense against pathogens. Sci Rep 2022;12(1):698. https://doi.org/10.1038/s41598-021-04700-y.
[29] Lu M, Gao Z, Xing S, Long J, Li C, He L, Wang X. Purification, characterization, and chemical modification of Bacillus velezensis SN-14 fibrinolytic enzyme. Int J Biol Macromol 2021;177:601–9. https://doi.org/10.1016/j.ijbiomac.2021.02.167.
[30] R S, J J, A TS. Purification, characterization, molecular modeling and docking study of fish waste protease. Int J Biol Macromol 2018;118:569–83. https://doi.org/10.1016/j.ijbiomac.2018.06.119.
[31] Sarkar S, Gupta S, Chakraborty W, Senapati S, Gachhui R. Homology modeling, molecular docking and molecular dynamics studies of the catalytic domain of chitin deacetylase from *Cryptococcus laurentii* strain RY1. Int J Biol Macromol 2017;104(Pt B):1682–91. https://doi.org/10.1016/j.ijbiomac.2017.03.057.
[32] Kiliszek A, Rypniewski W, Rząd K, Milewski S, Gabriel I. Crystal structures of aminotransferases Aro8 and Aro9 from *Candida albicans* and structural insights into their properties. J Struct Biol 2019;205(3):26–33. https://doi.org/10.1016/j.jsb.2019.02.001.
[33] Katrolia P, Liu X, Zhao Y, Kopparapu NK, Zheng X. Gene cloning, expression and homology modeling of first fibrinolytic enzyme from mushroom (*Cordyceps militaris*). Int J Biol Macromol 2020;146:897–906. https://doi.org/10.1016/j.ijbiomac.2019.09.212.
[34] Iraqui I, Vissers S, Cartiaux M, Urrestarazu A. Characterisation of *Saccharomyces cerevisiae ARO8* and *ARO9* genes encoding aromatic aminotransferases I and II reveals a new aminotransferase subfamily. Mol Gen Genet 1998;257(2):238–48. https://doi.org/10.1007/s004380050644.
[35] König S, Spinka M, Kutter S. Allosteric activation of pyruvate decarboxylases. A never-ending story? J Mol Catal B Enzym 2009;61(1):100–10. https://doi.org/10.1016/j.molcatb.2009.02.010.
[36] Alvarez ME, Rosa AL, Temporini ED, Wolstenholme A, Panzetta G, Patrito L, Maccioni HJ. The 59-kDa polypeptide constituent of 8-10-nm cytoplasmic filaments in *Neurospora crassa* is a pyruvate decarboxylase. Gene 1993;130(2):253–8. https://doi.org/10.1016/0378-1119(93)90427-5.
[37] Liu JB, Bai YJ, Fan TP, Zheng XH, Cai YJ. Unveiling the multipath biosynthesis mechanism of 2-phenylethanol in Proteus mirabilis. J Agric Food Chem 2020;68(29):7684–90. https://doi.org/10.1021/acs.jafc.0c02918.
[38] Crismaru CG, Wybenga GG, Szymanski W, Wijma HJ, Wu B, Bartsch S, de Wildeman S, Poelarends GJ, Feringa BL, Dijkstra BW, et al. Biochemical properties and crystal structure of a β-phenylalanine aminotransferase from *Variovorax paradoxus*. Appl Environ Microbiol 2013;79(1):185–95. https://doi.org/10.1128/AEM.02525-12.
[39] Yvon M, Thirouin S, Rijnen L, Fromentier D, Gripon JC. An aminotransferase from *Lactococcus lactis* initiates conversion of amino acids to cheese flavor compounds. Appl Environ Microbiol 1997;63(2):414–9. https://doi.org/10.1128/2Faem.63.2.414-419.1997.
[40] Bao WZ, Li X, Liu JF, Zheng R, Liu LJ, Zhang HB. The characterization of an efficient phenylpyruvate decarboxylase KDC4427, involved in 2-phenylethanol and IAA production from bacterial *Enterobacter sp*. CGMCC 5087. Microbiol Spectr 2022;10(2). https://doi.org/10.1128/spectrum.02660-21.
[41] Rzad K, Gabriel I. Characterization of two aminotransferases from Candida albicans. Acta Biochim Pol 2015;62(4):903–12. https://doi.org/10.18388/abp.2015_1158.
[42] Rząd K, Milewski S, Gabriel I. Versatility of putative aromatic aminotransferases from *Candida albicans*. Fungal Genet Biol 2018;110:26–37. https://doi.org/10.1016/j.fgb.2017.11.009.
[43] Hirata H, Ohnishi T, Ishida H, Tomida K, Sakai M, Hara M, Watanabe N. Functional characterization of aromatic amino acid aminotransferase involved in 2-phenylethanol biosynthesis in isolated rose petal protoplasts. J Plant Physiol 2012;169(5):444–51. https://doi.org/10.1016/j.jplph.2011.12.005.
[44] Xia HL, Shangguan L, Chen S, Yang Q, Zhang XL, Yao L, Yang SH, Dai J, Chen X. Rapamycin enhanced the production of 2-phenylethanol during whole-cell bioconversion by yeast. Appl Microbiol Biotechnol 2022;106(19–20):6471–81. https://doi.org/10.1007/s00253-022-12169-6.
[45] Stribny J, Romagnoli G, Pérez-Torrado R, Daran JM, Querol A. Characterisation of the broad substrate specificity 2-keto acid decarboxylase Aro10p of *Saccharomyces kudriavzevii* and its implication in aroma development. Microb Cell Factories 2016;15:51. https://doi.org/10.1186/s12934-016-0449-z.
[46] Liu S, Bai M, Zhou J, Jin Z, Xu Y, Yang Q, Zhou J, Zhang S, Mao J. Analysis of genes from *Saccharomyces cerevisiae* HJ01 participating in aromatic alcohols biosynthesis during *huangjiu* fermentation. Lebensm Wiss Technol 2022;154:112705. https://doi.org/10.1016/j.lwt.2021.112705.